

Classification of carbon nanostructure families occurring in a chemically activated arc discharge reaction

P.Dallas, S.S.Meysami, N.Grobert and K.Porfyrakis*

Received 00th January 20xx,
Accepted 00th January 20xx

DOI: 10.1039/x0xx00000x

www.rsc.org/

Controlling the generation of empty cage, endohedral metallofullerenes and carbon nanotubes is an important challenge for the tailored synthesis of functional materials and their scaled up production. However, the reaction yields for fullerenes are low and their formation mechanism is far from being elucidated thus hampering their targeted, scaled up synthesis and potential applications. We present a systematic study on the effect of the addition of copper nitrate as doping agent during an arc discharge vaporization of Gd and Nd doped rods for the production of a series of fullerenes and carbon nanotubes. The incorporation of copper nitrate at a Cu/M molar ratio in the range of 6 to 7 leads to higher yield for the high molecular weight fullerenes and endohedral fullerenes compared to small empty cages. We distinguished three different families of nanomaterials: 1) small empty cage fullerenes, 2) endohedral metallofullerenes and empty cage fullerenes with more than 88 atoms, and 3) multi-wall carbon nanotubes which were deposited on the cathode and their yield appeared to be influenced by the different reaction conditions.

Introduction

Metal encapsulating endohedral fullerenes (EMF) present an exciting class of materials. Unusual and improbable metal clusters or single metals can be trapped inside fullerene cages with various sizes and shapes thus creating materials with fascinating optical ^[1], magnetic ^[2] and electrochemical properties ^[3]. For example, mono-metallofullerenes such as Y@C₈₂ can be potentially used in quantum information processing devices due to the high spin lifetime ^[4] while the trimetallic nitride (TNT) type metallofullerenes are promising materials for a range of applications as magnetic resonance imaging contrast agents ^[5-6] or electron donors in solar cells due to their higher LUMO level compared to small empty cage fullerenes. ^[3]

However, the scaled up synthesis and applications of tailored fullerenes is still a major challenge due to the low overall yield of the current synthetic procedures, requiring violent conditions with high temperature and low pressure during an arc discharge reaction. The resulting mixture of fullerenes contains mostly C₆₀ and C₇₀ and their separation requires exhaustive chromatographic separation techniques or selective reaction of the metallofullerenes with Lewis acids like TiCl₄. ^[7] Furthermore, there is currently no established formation mechanism which could be exploited for designing experiments to maximize the yield.

Whilst using the arc discharge, a number of methods have been developed in order to address this challenge, which often

involve the use of reactive gases, e.g. NH₃ ^[8], or the doping of the electrodes with solid organic compounds such as calcium cyanamide ^[9], not all nanostructures have been isolated. For example, in 2007, Stevenson et al. ^[10] first reported the now widely adopted CAPTEAR method ("Chemically Adjusting Plasma Temperature, Energy and Reactivity") and showed that filling the core of graphite/Sc₂O₃ electrodes with copper nitrate ^[10] or metallic Cu ^[11] resulted in the selective formation of TNT type metallofullerenes, e.g. Sc₃N@C₈₀, which form preferentially against empty cage fullerenes. They claimed that when the amount of dopant reached 80% wt, from the 13 mg of extracted fullerenes, the 12 mg were identified as TNT Sc₃N@C₈₀ while the yield of C₇₀ exceeded the yield of C₆₀ with 90 % wt dopant. During this arc discharge vaporization process, copper nitrate decomposes and forms nitrogen gases and vaporized copper that influence the temperature, energy, arc conductivity and reactivity of the plasma atmosphere inside the arc chamber. However, Stevenson et al. ^[10] and Yang et al. ^[9] used only aromatic hydrocarbons, such as o-xylene or toluene, for the extraction of the fullerenes from the as produced soot, and hence are likely to have overlooked a number of metallofullerenes which tend to dissolve in polar solvents for instance dimethylformamide (DMF) and they do not study the effect of applied current on the synthesis of both fullerenes and nanotubes.

The other major class of carbon nanostructures that are formed during an arc discharge process is the carbon nanotubes (CNTs). ^[12-14] CNTs are typically found in cathode deposits ^[15] while fullerenes are equally distributed in the fine powdered soot ^[16], and are embedded in a carbon matrix totally non dispersible in common solvents. The mechanism of formation of CNTs in arc discharge has been suggested to be quite different from the small and spherically shaped fullerenes and involves either an ion flow and diffusion on the cathode electrode, typically through the arc discharge centreline where the plasma density has its highest value, which is the bottom up

^a Department of Materials, University of Oxford, OX1 3PH, UK.

*Kyriakos.porfyrakis@materials.ox.ac.uk

† Information on the characterization techniques, a table with quantitative reaction yields, detailed mass spec for and additional SEM and TEM images are available free of charge via the internet.

See DOI: 10.1039/x0xx00000x

approach^[17] or a folding of the graphene layers, the top down route.^[18] The latter has been demonstrated in the spontaneous transformation of graphene to carbon nanostructures upon heating.^[19] In our work, the formation of these carbon nanomaterials using a chemically activated arc-discharge was studied and compared to counterpart techniques such as chemical vapor deposition (CVD) in order to have a better picture on the reaction conditions and the interplay and competition between the formed conjugated nanoclusters stemming from the same graphite vaporization route.

We alternated the applied DC current, helium pressure as well as the molar ratio between $\text{Cu}(\text{NO}_3)_2 \cdot 3\text{H}_2\text{O}$ and the rare earth metals (Gd - Nd) and consequently the plasma density in order to efficiently construct a model for the formation of the various structures that can be identified and isolated. We identified the presence of distinguishable families of nanomaterials that follow interconnected formation pathways during their synthesis and can be further used in order to elucidate the formation mechanism of the fullerenes during an arc discharge process and lead to rational design of experiments. The addition of copper nitrate not only provides a reactive nitrogen and oxygen source but also alters the conditions of the arc discharge process by increasing the local temperature and the plasma reactivity and density thus leading new reaction paths for the formation of fullerenes and carbon nanostructures.

2. Experimental section

The arc discharge reactor was evacuated at a pressure of 3×10^{-4} Torr and then filled with He gas. Experimental conditions were optimized for the production of fullerenes [200 amps direct current, 50 mbar] and carbon nanotubes [80 amps/450 mbar]. The graphite rods were doped with Nd_2O_3 or Gd_2O_3 (Toyo Tanso, 2 % wt. Gd_2O_3 , rod density: 1.869 g/cm³; and 1.6 % wt. Nd_2O_3 , rod density: 1.653 g/cm³).

For the copper nitrate doping, the rods were core drilled in the dimensions 2 mm × 5 cm and 2.7 mm × 5 cm and filled with powdered $\text{Cu}(\text{NO}_3)_2 \cdot 3\text{H}_2\text{O}$ (Sigma Aldrich) and subsequently vaporized as the anode. The molar ratio between $\text{Cu}(\text{NO}_3)_2 \cdot 3\text{H}_2\text{O}$ and Gd_2O_3 or Nd_2O_3 was 1.98 and 2.37 and 6.274 and 7.11 respectively. The rods were refilled with the copper nitrate after a few arcs due to evaporation of the later. The vaporization of the copper nitrate rods was visibly faster compared to the non-doped rods under the same conditions indicating the significantly higher temperatures during the reaction. The following abbreviations are used to represent the copper doping and the reaction conditions, X: no copper added, A: Cu/M molar ratio 1.98 (Gd) or 2.37 (Nd); B: Cu/M molar ratio 6.27 (Gd) and 7.11 (Nd); 1: 200 amps, 50 mbar; 2: 80 amps, 450 mbar.

In all cases, the yield of the fullerenes corresponds to the same amount of carbon soot, 17 g, and the fullerenes were extracted in two stages with two different solvents. In the first step the soot was extracted with toluene for 90 hours and in the second step with dimethylformamide (DMF) again for the same time, 90 hours in order to ensure complete removal of all fullerenes, since the more polar metallofullerenes can be easier extracted with DMF. The fullerenes were isolated from the extract by high performance liquid chromatography (HPLC) and further characterized with mass spectrometry.

The robust carbon deposit, forming on the cathode and containing CNTs was carefully removed, to avoid contamination

from the soot, for subsequent characterization. Detailed information on the characterization techniques is provided in the Supporting information section.

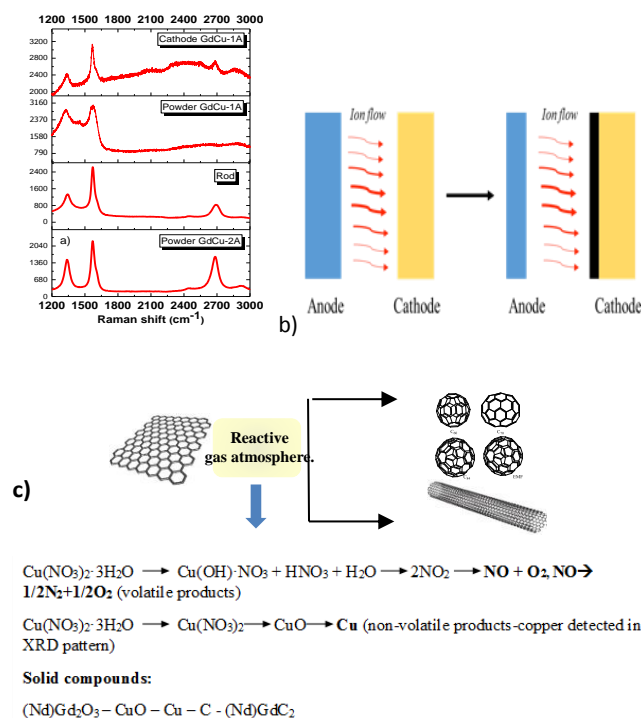


Fig. 1. a) Raman spectra of: Pristine graphite rods, fine powder for GdCu-1A, cathode deposit for GdCu-1A and powder for GdCu-2A. b) Schematic representation of the arc discharge reaction indicating the decomposition products of (c) copper nitrate and the structures formed either inside the fine powdered soot or in the cathode deposits.

3. Results and discussion

3.1. Synthesis and reaction conditions.

An arc discharge reaction is a violent process that generates a wealth of products that are embedded in a carbon matrix. Small molecules, fullerenes and carbon nanotubes are all formed from the collision of the carbon fragments and metal ions in the arc plasma. Due to the complexity of the process there is a debate concerning the formation mechanism of the fullerenes and the conditions affecting their synthesis.

In our work we altered the reaction conditions based on the doping of the graphite rods with copper nitrate. Based on the different reaction conditions, we obtained different reaction yields for various empty cage and endohedral fullerenes. The decomposition of this doping agent generates reactive gases including oxygen and nitrogen oxides and as an exothermic process it leads to a substantial increase of the local temperature. Despite the fact that the process is taking place under an inert Helium atmosphere, there is still presence of oxygen from the gadolinium oxide, the water molecules of the copper nitrate and the NO_3 units. The thermal decomposition of

the copper nitrate under vacuum [20] and under inert atmosphere has been extensively studied in the past with exothermic peaks observed in differential scanning calorimetry analysis [21]. According to these early works we outline the decomposition products in Figure 1c. Ding et al [21] employed Differential scanning calorimetry to study the decomposition of copper nitrate and they observed four peaks at 107, 126, 225 and 305 °C. They assigned them to different weight losses on the TGA graphs and they claimed that the copper oxide that is formed in lower temperatures, close to 310 °C catalyses the further decomposition of nitric acid to nitric oxide and nitrogen oxide. An extensive study on the thermal decomposition of metal nitrates, the enthalpies of the reaction and the volatile products can be seen in the work by Stern. [22] It is well known that the decomposition of NO₂ and NO are exothermic processes with an enthalpy of 33.2 kJ/mol and 90.29 kJ/mol respectively. Thus from the decomposition of NO₂ we expect to have an energy release of 0.13 kJ and 0.35 kJ for the lower and the higher copper loading respectively in each rod. This decomposition subsequently releases oxygen, where the enthalpy of carbon oxidation is 394 kJ/mol initiating further exothermic reactions. This is inherently a combustion process as used previously for the CAPTEAR method. The gaseous molecules are increasing the local pressure approximately 8 times according to the work by Morozov et al [23]. These gases are expected to alter the reactivity of the plasma and consequently the products of the collision of small carbon fragments towards symmetric fullerenes. Furthermore, the formation of oxygen will lead to more exothermic reactions in the hot plasma. This is of particular importance since a metal-carbon plasma plume is the source of both the empty cage and endohedral metallofullerenes.

A first look in the graphite rods used for the arc discharge process is demonstrating a partial graphitization signalled by the strong D-band and the relatively broad G-band in the Raman spectrum (Fig. 1a, sample GdCu-1A). After the arc discharge reaction we distinguish between the fine powdered carbon soot randomly distributed in the reactor that contains the fullerenes and the robust cathode deposit that contains the carbon nanotubes. Their Raman spectra are strikingly different with the fine powder exhibiting a completely disordered structure marked with the absence of a G' band, a weak and broad G band and a strong D band while the cathode deposit appears more graphitized than the initial carbon rods. Here we note that G' band is observed in defect free graphitized samples. [24]

3.2. Extraction and separation of the fullerenes: HPLC analysis

The fractions were isolated by HPLC using toluene as eluent. Fig. 2 shows the chromatographs of the crude extracts for toluene and DMF Soxhlet extractions for both the Gd and Nd samples. The fullerenes eluted according to their retention time and, as expected, the empty cage fullerenes with lower molecular weight eluted faster than the endohedral metallofullerenes and the amount of small empty cage fullerenes observed in the chromatographs for the second stage DMF extraction was negligible.

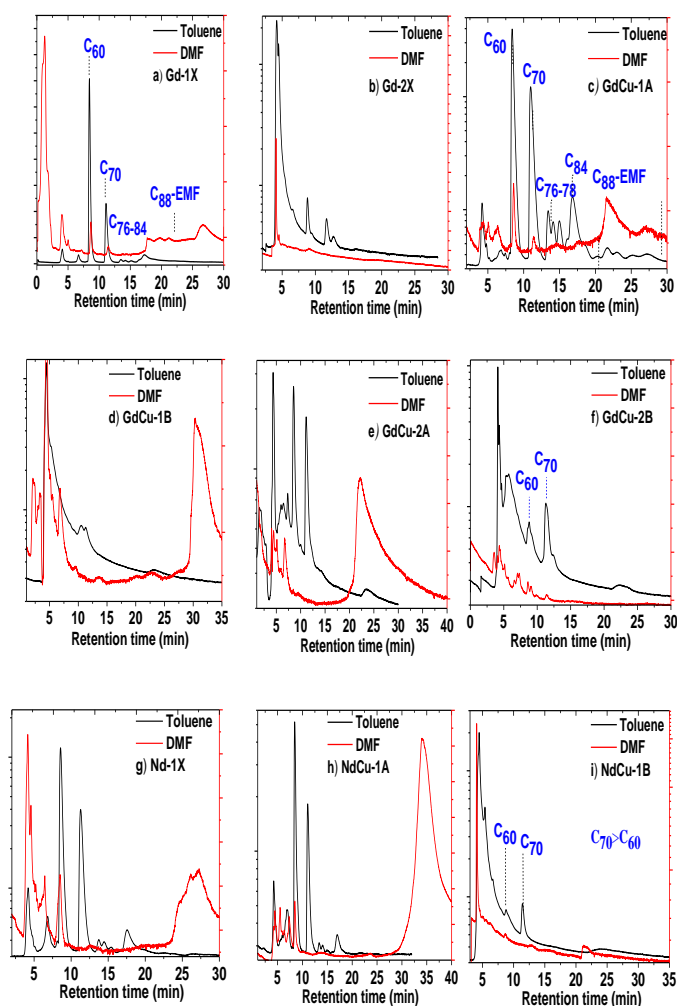


Fig. 2. HPLC graphs of the crude soot extract derived from the vaporization of graphite rods for the Gd (a-f) and Nd (g-i) samples. Both extraction steps are presented. Black line: toluene extraction. Red line: DMF extraction.

We distinguish three different areas in the HPLC graphs that correspond to specific classes of fullerenes. In the first class we place the high yield small empty cage fullerenes, C₆₀ and C₇₀, in the second the lower yield, empty cage, C₇₆₋₈₄, and finally the fullerenes that appear at very high retention times, higher than 22 min.

The Gd-1X and Nd-1X samples demonstrate the common trend of the fullerene formation during an arc discharge reaction with the C₈₄ to be the third most abundant fullerene. The GdCu-1A/NdCu-1A samples that were synthesized in the presence of copper nitrate are showing the same trend for cages between 60-84 carbon atoms however the peaks at higher retention times are significantly more intense compared to the Gd-1X/Nd-1X. For GdCu-1B, GdCu-2B and GdCu-2A, the C₈₄ peak is noticeably missing, meaning that the conditions of low current and high pressure and the very high molar ration of Cu/M do not favour the formation of these structures. Furthermore, even the C₆₀-C₇₀ fullerenes that normally appear

with very high yield were totally suppressed on the reactions with Cu/M ratio between 6 and 7 in accordance with previous observations by Stevenson et al.

In all cases, the region were the EMFs and higher fullerenes appear is either a broad peak (signaling the formation of different isomers or fullerenes with strongly correlated structures) or a series of weak peaks. Mass spectrometry was employed to confirm whether endohedral metallofullerenes or very large carbon cages were formed and the full spectra can be found in the supporting information (Fig. S1-S13).

3.3. Mass spectroscopy: identification of the higher and endohedral metallofullerenes products.

We summarize our mass spectrometry findings in Figure 3, Table I. The most abundant endohedral metallofullerene for the Gd-1X sample is the well-known Gd@C₈₂ EMF ($m/z=1142$). When copper nitrate was added in a molar ratio Cu/Gd 2:1 Gd@C₈₂ appeared with low intensity in the mass spectrum. In this case we observed a series of large cage fullerenes, namely C₉₀₋₉₈ (m/z 1080-1177) and Gd@C₉₀ ($m/z=1238$). In reaction conditions involving lower DC current, the bimetallic fullerenes Gd₂@C₈₀₋₉₀ appear with high intensity. Large bimetallic fullerenes like Gd₂@C₉₀ ($m/z=1396$) have already been reported by Yang et al. [25] and should be expected to be formed in our experiments due to the very high Gd loading of the rods (2 % wt). Interestingly, we observe that only Gd leads to bimetallic fullerenes under these conditions while Nd leads exclusively to monometallic clusters, i.e. Nd@C₈₀₋₈₄ ($m/z=1104-1152$). Trimetallic type metallofullerenes were observed only in the case of high copper-metal molar ratio, between 6 and 7 for both Nd and Gd. The mass spec indicating the formation of Gd₃N@C₈₀ and Nd₃N@C₈₂ for the samples GdCu-1B and NdCu-1B are shown in Fig. 3. This means that only in this case we have sufficient amounts of nitrogen in order to form TNT EMFs.

Sample name	Fullerene (m/z)
Gd-1X	Gd@C ₈₂ ($m/z=1142$)
Gd-2X	Gd ₂ @C ₈₀ (1276), Gd@C ₈₂ (1142)
GdCu-1B	Gd ₃ N@C ₈₀ (1447), Gd ₂ @C ₈₀ (1276), Gd@C ₈₂
GdCu-1A	C ₉₀ -C ₉₈ (1080-1177)
GdCu-2A	Gd ₂ @C ₈₄₋₈₈ (1324-1372)
Nd-1X	Nd@C ₈₀₋₈₄ (1104-1152)
NdCu-1B	Nd ₃ N@C ₈₂ (1430)
NdCu-1A	Nd@C ₈₀₋₈₂

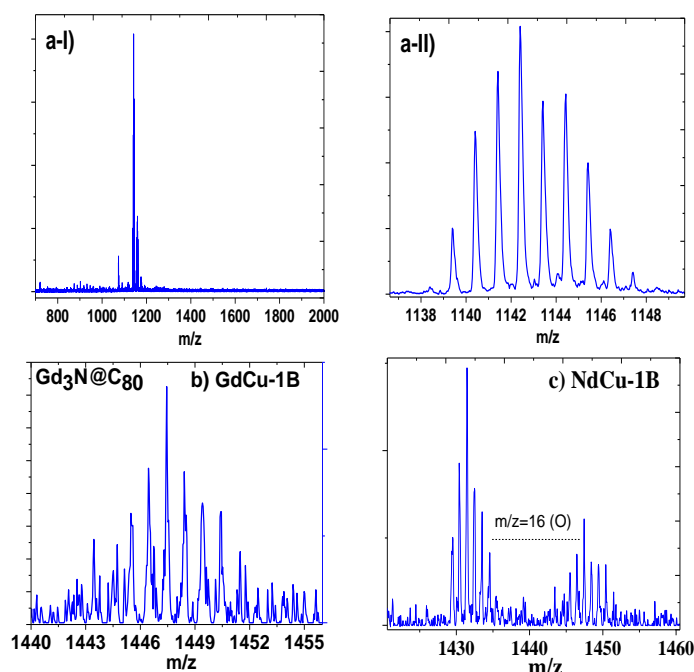


Fig. 3. In Table 1 we present the identified EMFs and higher fullerenes (>C₈₈) observed in different reaction conditions. a) Full mass spectra for the Gd-1X sample. Retention time: 23-26 min, positive ionization. A magnification of the m/z range corresponding to the Gd@C₈₂. Typical mass spectra for b) TNT, Gd₃N@C₈₀ (c) and Nd₃N@C₈₂ fullerenes.

3.4. Interplay between the different fullerenes and their reaction yields

In order to construct a map of the fullerene formation under CAPTEAR conditions we focus on the overall yields of the fullerenes summarizing the amounts obtained from both the toluene and the DMF extractions (see Figure 4). In our discussion we totally exclude the possible formation of the insoluble “missing small band gap metallofullerenes” like M@C₆₀, that the Shinohara group managed to isolate by surface functionalization with perfluorinated carbon groups. [26]

The reaction yields were calculated by using calibration curves based on the area of the peaks at the HPLC graphs. Exact yields are provided on Table S1 in the supporting information section. In Fig. 4a-b we are plotting the mass of each fullerene product in a logarithmic scale, with (a) for Gd and (b) for Nd. By carefully looking at the plots there is an apparent picture that the yields of all fullerenes are following a similar trend and function when no copper nitrate is added (Gd-1X and Nd-1X), which demonstrates that we are able to completely extract these reaction products and that the fullerenes followed a similar formation path independent of the rare earth metal and the density of the rods. When copper nitrate is added in a Cu/Gd ratio of 2 and the conditions are kept at 200 Amps and 50 mbar He pressure, a similar trend is observed only for the empty cages fullerenes C₆₀₋₈₄, while the yield of the higher and EMFs surpasses the one for C₈₄ meaning that the arc discharge conditions are becoming more favorable for EMFs and high fullerenes.

In the first family of carbon nanostructures we place the high yield C₆₀ and C₇₀ and in the second the empty cages C₇₆₋₈₄. C₆₀ is the most favourable structure during the arc discharge

vaporization process and this is observed in all samples with the striking exceptions to be GdCu-1B, GdCu-2B and NdCu-1B. In this case, the Cu/M molar ratio has the highest value and is 6.2 and 7.1 respectively, meaning that a very large amount of reactive gases is produced and an increase of the arc temperature took place. It is interesting to notice here that in our experiments C_{84} was not observed for either of the Gd and Nd samples with high molar ratio of copper nitrate and in fact, in both cases the C_{70} and even the C_{76-78} surpasses the yield of C_{60} . The reason behind this unusual behaviour and the exact mechanism of this phenomenon cannot be elucidated at this point and is beyond the scope of this work. However, since in previous works has been demonstrated that C_{70} requires higher temperature for formation compared to the C_{60} and is thermodynamically favoured while C_{60} is kinetically favoured, this can be a strong indication of more extreme conditions taking place in our activated plasma arc discharge. [27] Under a typical arc discharge experiment the C_{60} : C_{70} ratio is close to 3:1 and indeed this is what we observe without the presence of any dopants in both neodymium and gadolinium doped rods. This picture dramatically changes though upon doping and we summarize these findings in the detailed contour mapping of Fig. 5.

The fact that in both the Gd and Nd cases at the highest Cu/M molar ratio we observe a substantial suppression of these two small empty cage fullerenes while the yield of the EMFs and high empty cage fullerenes with cages larger than 88 carbon atoms was higher even than C_{60} means that this behaviour is independent of the rare earth metal incorporated in the rods. Both neodymium and gadolinium in fact donate three electrons to the carbon cage. In previous studies on the synthesis of trimetallic nitride scandium EMFs, the incorporation of a small amount of nitrogen or ammonia gas in the chamber resulted in a substantial increase of metallofullerenes, specifically $Sc_3N@C_{80}$, again surpassing the yield of C_{84} . [28] The selective synthesis of nitride fullerenes instead of monometallic by Stevenson [10] proves that the dramatic change in the reaction yields arises from the nitrogen containing dopant and not from different current density due to a change in the cross sections from the drilled anodes.

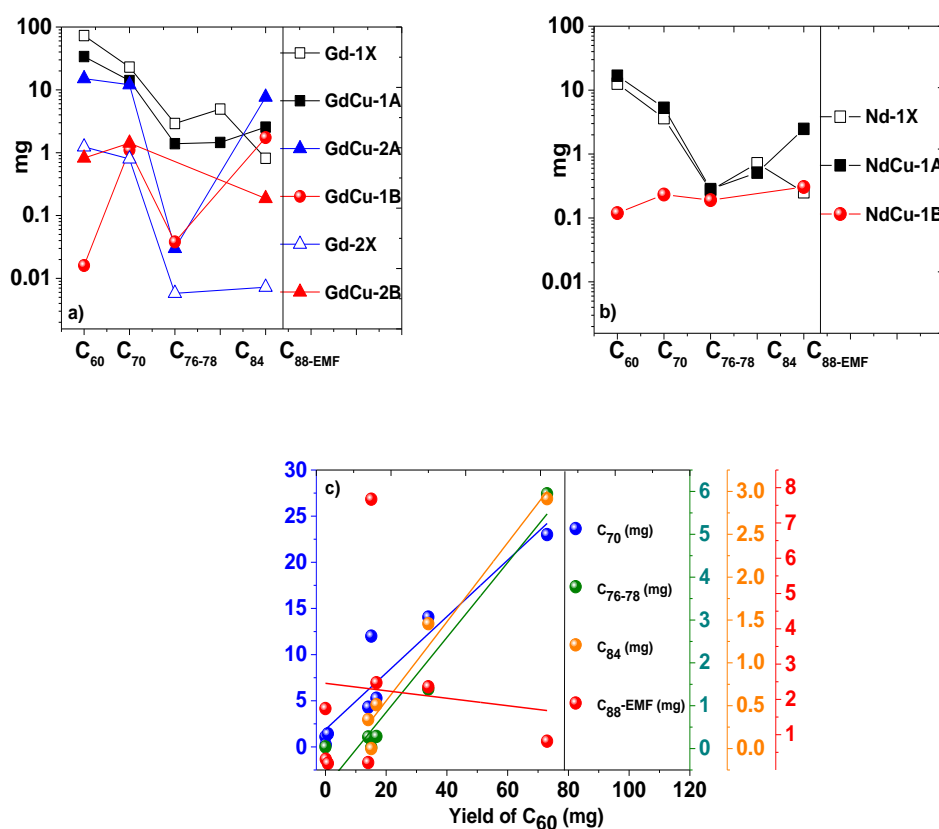


Fig. 4. a-c) Summary of the reaction yields of all the empty cage and endohedral metallofullerenes that could be isolated with HPLC and identified by mass spectroscopy. The Y axis representing the yield in mg of each product is in logarithmic scale due to different orders of magnitude between the empty cage lower fullerenes and endohedral metallofullerenes. c) The yield of C_{70} , C_{76-78} , C_{84} and C_{88-EMF} is presented against the yield of C_{60} .

In Fig. 4c we present the yields of C₇₀-C₇₆₋₇₈-C₈₄-C₈₈-EMF against the yield of empty cage C₆₀ for all samples. We include data for both types of rods even if according to Yang et al the slightly higher ionic radii of the Nd³⁺ compared to Gd³⁺, namely 0.995 Å compared to 0.95 Å has the inverse influence on the overall yield of EMF. [29-30] A recent work by the groups of Kroto and Shinohara demonstrated that the formation of metallofullerenes is directed by a three electron charge transfer between the metal ion and the carbon clusters and is a universal property, independent on the metal that is used. [31] They proved that the formation of large cage EMFs is further stabilized by nucleophilic attack through C₂ ions in a dominant bottom up process. Furthermore, the influence of doping agents in the formation mechanism of fullerenes is not universal and different metals behave with distinctive way. As an example S. Yang et al [32] synthesized the improbable fullerene YCN@C₅(6)-C₈₂ and observed that the addition of TiO₂ in the raw mixture of metals and graphite was essential for the synthesis of this fullerene. However when the same conditions were applied in the presence of Tb₄O₇ instead of Y₂O₃ it was found that titanium oxide was not essential for the formation of TbCN@C₅(6)-C₈₂ signalling different reaction pathways depending on the ionic radius and reactivity of each rare earth metal. [33]

In Fig. 4c we see that while the linear fitting for the C₇₀-C₇₆₋₇₈-C₈₄ reaction yields is demonstrating that the amount obtained from these fullerenes increases proportionally with the yield of C₆₀, in the case of C₈₈-EMF class, the trend is inverted and the higher the yield of C₆₀, the lower the yield of C₈₈-EMF suggesting a competing formation mechanism between the two families of fullerenes. The fact that the yield of very high cages is increased alongside the yield of EMFs is not surprising since rare earth metals need a large cage to be incorporated. On the hand the difference between this family and the class of C₆₀-C₇₀ suggests a competing formation mechanism, implying that the dense plasma atmosphere preferentially leads to the formation of cages larger than the so-called missing link C₈₄ proposed by Dorn et al.

The above observations enable us to construct a phase diagram on the formation of the fullerenes according to the applied current and the Cu/M molar ratio. For clarity we divide the yield of C₈₈-EMF with the sum of the yields of both the C₆₀ and C₇₀ since in specific samples the yield of C₇₀ surpasses the yield of C₆₀. In Figure 5a we present this relative yield compared to the Cu/M molar ratio and applied current for all samples. This diagram also indicates that the very dense plasma atmosphere due to the high concentration of Cu(NO₃)₂ leads to preferential formation of large cage fullerenes and metallofullerenes. Even if the exact temperature conditions for fullerene formation cannot be exactly identified, many authors claim a temperature of 4000 °C in the centre of the arc and a formation of fullerenes in a small distance from it (2-3 mm) with the optimum temperature for their growth to be in the range of 2000-2500 °C. The most interesting feature of the diagram lies in the fact that extreme conditions of high current, high temperature and plasma density totally suppress the formation of C₆₀-C₇₀ and favor the formation of bigger cage fullerenes, with the yield of the later to becoming higher than the former in specific conditions. [34] By taking into account the exothermic decomposition of copper nitrate that will locally increase the arc temperature and pressure we conclude in a different conditions for the preferential formation for small cage vs large cage/EMF,

however no quantitative data on the temperature and the pressure range is possible to be given. While other factors can be taken into account regarding the formation of the fullerene families, as for example the intense ultraviolet radiation from the center of the arc plasma, [35] our experimental set up is not enabling the further study of this parameter. It cannot be excluded though that the transition metal and nitrogen compounds to have a totally different spectrum that results in the excitation of the fullerenes to the triplet state, an open shell configuration that subsequently reacts with other carbon species and small C₂ fragments. [36]

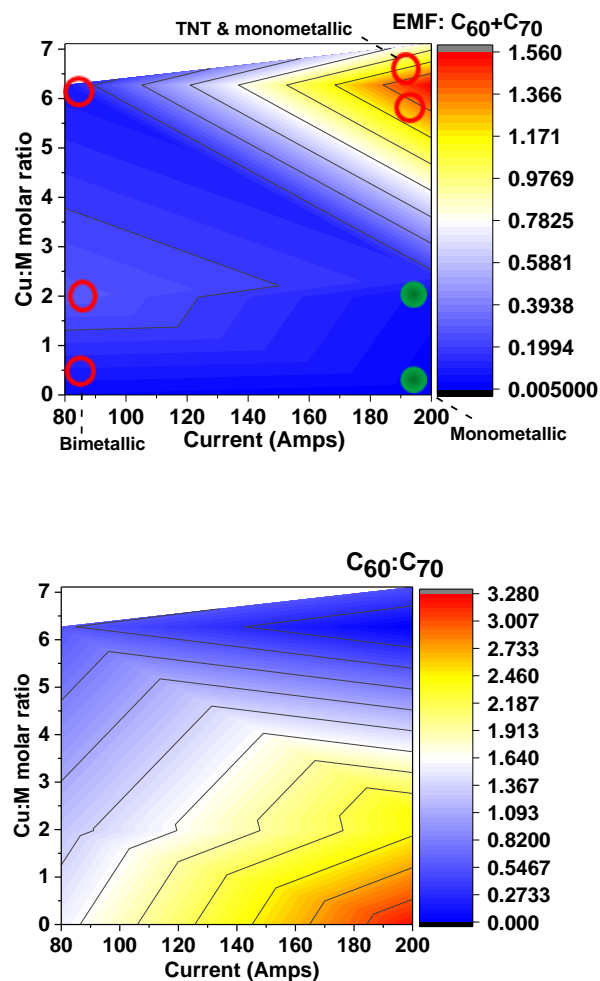


Fig. 5. A detailed mapping of the reaction. Contour map: X axis: DC current (Amps), Y axis: Cu/M molar ratio (M: Gd or Nd), Z axis: Ratio of the reaction yields of the C₈₈-EMF and (C₆₀+C₇₀) for (a) and C₆₀ to C₇₀ for (b). Green spheres indicate the conditions of an experiment where C₈₄ was observed; Red circles: C₈₄ could not be detected under these conditions.

3.5. Carbon nanotubes formation: dependence on the reaction conditions.

In Fig. 1 we demonstrated that there are two different routes that the carbon fragments can follow in order to re-

arrange themselves after the vaporization [37–38]: in the first case, small fragments accumulate to form spherically shaped conjugated carbons thus minimizing the energy of the cluster, i.e. fullerenes. These spherical nanomaterials are embedded in a highly disordered amorphous carbon phase, while in the second case, the ion flow towards the cathode results in elongated carbon nanotubes embedded in a dense, solid and non-dispersible in common solvents matrix. No fullerenes could be extracted by the cathode deposit neither with toluene nor DMF.

There are various bottom-up or top down mechanisms proposed for the synthesis of fullerenes, involving even some unconventional routes like the heptagon road. [36, 39] Recently the top down approach has been also proposed suggesting a folding of graphene layers that fold to form either carbon nanotubes or low symmetry metastable fullerenes. These metastable fullerenes by losing C_2 groups are forming the common high symmetry derivatives that are routinely extracted with organic solvents. The unique asymmetric $C_{1(51383)}-C_{84}$ cage that exhibits destabilizing fused pentagons was proposed as a link in the formation of high and endohedral fullerenes from the metastable fullerene structures. [40] Zhang et al suggested that C_{84} rearranges to more stable structures at higher temperatures by elimination of pentalene and pyracetylene motifs. [40] They used ^{13}C carbon in order to mark the different reaction pathways and intermediates towards the formation of yttrium metallofullerenes. The fact that C_{84} can indeed be a boundary between different structures is following our observations with the C_{84} to be a border between the two other classes of fullerenes. Interestingly in the samples that proved to have the largest and highest quality network of nanotubes the C_{84} fullerenes were either missing, namely GdCu-2A or they had much lower yields than EMFs like in the GdCu-1A. However, Dunk et al demonstrated through the closed network growth of fullerenes that C_{60} is following a bottom up route, and is formed from small clusters instead of breaking down of large cage fullerenes like in top down mechanism. These small and highly reactive species react with hydrogen and oxygen thus their formation is highly suppressed under such conditions. [31]

Fig. 6 presents SEM images of four different deposits where we were able to identify carbon nanofibers and nanotubes. We chose for our study the samples Gd-1X (Figure 6a–b), GdCu-1A (Figure 6c–d), GdCu-1B (Figure 6e–f) and GdCu-2A (Figure 6g–h). The SEM images from the Gd-1X are demonstrating the formation of a limited number of nanofibers with a diameter of 100 nm embedded in a carbon matrix. The conditions of the experiment were optimized for fullerenes, i.e. high current and low pressure. Interestingly, when we incorporated copper nitrate inside the rods, we were able to observe a fine network of carbon nanotubes (GdCu-1A, and GdCu-2A, both with Cu/M molar ratio 2). It is interesting to notice here that unlike iron [41–42], nickel and cobalt [43], metallic copper has never been considered an efficient catalyst for multi-wall carbon nanotubes (MWCNTs) growth during chemical vapour deposition (CVD) [44] process despite the few reports on the formation of fine single-wall carbon nanotubes (SWNTs) in a copper catalysed system. [45] In general for CNT growth an ineffective catalyst is due to the absence of a significant solubility of carbon in the metal or because stable carbides are formed at high carbon concentrations. For example in systems like carbon–copper, carbon–zinc, carbon–gadolinium, and carbon–cadmium systems, the solubility limit of carbon in the metals is extremely

low (0.0001 wt.% C in Cu at 1100 C) [46]. Carbon cannot diffuse in sufficient amounts into the nanoscale catalyst particles and these particles cannot act as nucleation sites for the formation of carbon nanotubes. Concerning the formation of fibrillar large diameter structures in this sample the presence of a Gd in the electrode might have promoted the catalytic growth of carbon fibers as also CNTs as suggested by Wierczewska et al. [47]. The two samples with a Cu/M molar ratio of 2 (GdCu-1A and GdCu-2A) demonstrated the synthesis of an extensive network of carbon nanotubes. No significant differences were observed in the diameter of the nanotubes between these two samples. In the experiment with the highest molar ratio of copper nitrate, sample GdCu-1B, totally linear and long nanotubes were formed without the curly structures observed in the three other samples. However, their yield was much lower compared to the other two samples. It is interesting to notice that in this case, the GdCu-1B sample, is the one that demonstrates the highest EMF/($C_{60}+C_{70}$) ratio.

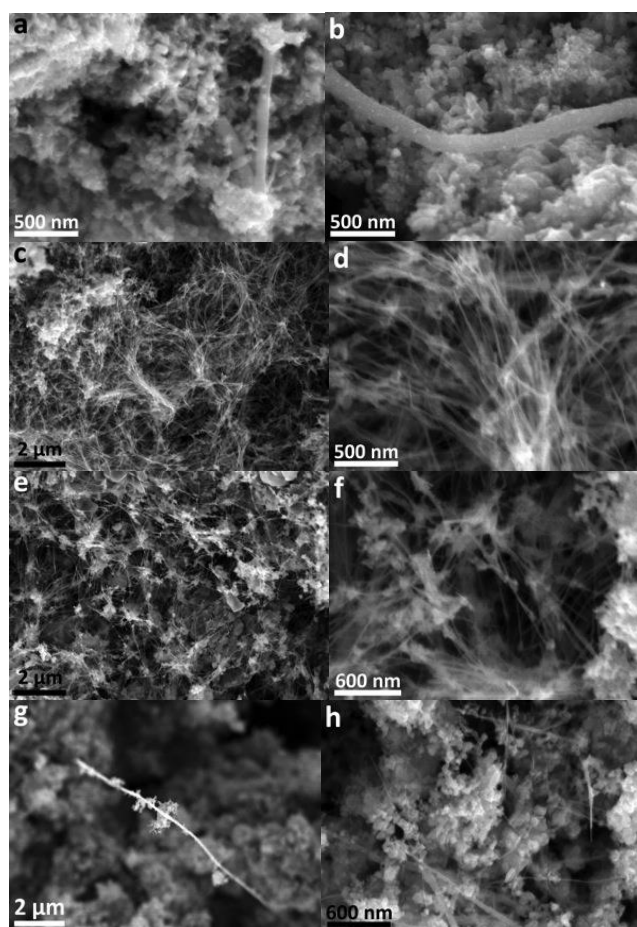


Fig. 6. SEM images of the carbon nanotubes and nanofibers obtained from the cathode of the arc discharge reactor. The samples are a–b) Gd-1X c–d) GdCu-1A e–f) GdCu-2A g–h) GdCu-1B

The XRD pattern (Fig. 7a) of the cathode deposits demonstrate the presence of gadolinium carbide nanoparticles, GdC_2 , in both the GdCu-1B and GdCu-2A with a mean crystallite size estimated by Scherrer equation to be 14 nm. Interestingly the XRD pattern demonstrates the presence of metallic Cu in the GdCu-2A samples as derived from the vaporized anode. This

could be seen in the remaining graphitic anode with the rod having a characteristic copper color. Even if the whole process is very complex and difficult to elucidate the reaction mechanism it is strongly supporting a reducing atmosphere during the arc discharge vaporization process similar to the thermal analysis studies of copper nitrate. In contrast metallic copper was not detected in the XRD patterns of the GdCu-1B sample (Fig. 7a). Here we have to notice that the boiling point of copper is 2562 °C and the melting point of Gd_2O_3 is 2420 °C. This is a strong indication of a significant difference in the local temperature and the conditions upon addition of higher amount of copper nitrate.

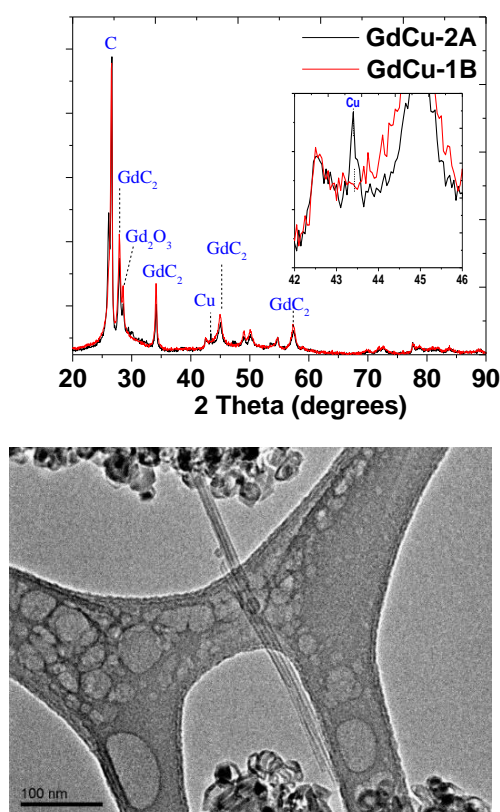


Fig. 7. a) XRD patterns for GdCu-2A and GdCu-1B samples. Metallic copper is observed in GdCu-2A. The size of the gadolinium carbide crystallites is estimated to be 14 nm as calculated from the Scherrer equation b) TEM image of GdCu-1A sample. The database assignment for the XRD peaks can be seen in Figure S17.

Finally, the exact size of the CNTs was confirmed by TEM analysis (Fig. 7b), demonstrating the presence of MWCNTs embedded in an amorphous carbon matrix and inorganic nanoparticles with the average outer diameter of the MWNTs to be estimated around 20 nm. The dark particles embedded in a carbon matrix are most probably the gadolinium carbides and their formation has been already reported in previous publications on the arc discharge of various metal oxides. [48-49]

3. Conclusions

Copper nitrate doping is found to significantly influence the formation of different carbon nanostructures during the direct current, arc discharge vaporization of graphite rods. By carefully studying the reaction yields of the fullerenes and the morphology of the carbon nanotubes we conclude in the formation of three distinctive but interconnected families of nanostructures: Empty cage lower fullerenes (C_{60-84}), higher fullerenes with more than 88 carbons alongside EMFs and the 1-D nanostructures, i.e. nanofibers and nanotubes formed in the cathode. In this methodology the temperature, the reactive gas atmosphere and the plasma density can be tuned according to the reaction conditions and the doping level of the graphite electrodes. The presence of reactive gases due to the decomposition of copper nitrate, coupled with the fact that this is an exothermic process, is found to influence not only the yield of the endohedral metallofullerenes but also the size, shape and graphitization of the elongated carbon nanostructures, namely nanotubes and fibers. These findings enable us to construct a picture on the formation mechanism of the various carbon nanostructures. This is crucial for the further development of targeted synthetic methods for novel fullerenes with exciting new properties. **Mixed metal metallofullerenes have been more difficult to be synthesized compared to the monometallic and TNT EMFs and the type of inorganic cluster trapped inside the fullerenes and the simultaneous formation of carbon nanotubes is dictated by thermodynamic factors, the effective collisions of plasma ions and the formation of charge transfer complexes between the metal and the cage as proven by Shinohara and Kroto. [31] To that end, we constructed maps of current vs doping ratio where the favoured formation of monometallic, bimetallic or very large empty cage fullerenes is outlined. Considering the bottom-up insertions of C_2 as the most possible formation mechanism this may be controlled by adding reactive small dopant molecules and changing the reaction conditions. This is further indicated by the reverse in the yields of the C_{60} and C_{70} , with the latter to have a lower heat of formation. [27] Finally, by reducing the extracted amount of the otherwise abundant $\text{C}_{60}/\text{C}_{70}$ empty cage fullerenes, not only conventional purification methods like HPLC, but newer methods like Lewis acid separation may be easier to be scaled up since the hindrance of oversaturated crude extracts will be overcome.**

Supporting information: Information on the characterization techniques, a table with quantitative reaction yields, detailed mass spec for and additional SEM and TEM images are available free of charge via the internet.

Acknowledgements. We acknowledge EPSRC funding for the Fellowship programme ‘manufacturing the future: endohedral fullerenes, small molecules, big challenges’ (EP/K030108/1). We acknowledge the EPSRC UK National Mass Spectrometry Facility, College of Medicine, Swansea University for recording the mass spectra and Dr Phil Holdway for recording the XRD patterns. We are also grateful for the financial support received from the European Community’s Seventh Framework Programme (FP7/2007–2013): the Marie Curie CONTACT Project under grant agreement no. 238363; The Royal Society, European Research Council (ERC) Starting Grant (ERC-2009-StG 240500 DEDIGROWTH; and ERC-2012-PoC 309786 DEVICE); UK

Government for Engineering and Physical Sciences Research Council (EPSRC) Pathways to Impact grants.

References

1. S.Bandow, H.Kitagawa, T.Mitani, H.Inokuchi, Y.Saito, H.Yamaguchi et al. *J.Phys.Chem.* 1992, **96**, 9609-12
2. F.Hajjaj, K.Tashiro, H.Nikawa, N.Mizorogi, T.Akasaka, S.Nagase. et al. *J.Am.Chem.Soc* 2011, **133**, 9290-9292
3. RB.Ross, CM.Cardona, DM.Guldi, SG.Sankaranarayanan, MO.Reese, N.Kopidakis. et al. *Nature Materials* 2009, **8**, 208-212.
4. RM.Brown, Y.Ito, JH.Warner, A.Ardavan, H.Shinohara, GAD.Briggs. et al. *Phys. Rev. B.* 2010, **82**, 033410-4
5. H.Kato, Y.Kanazawa, M.Okumura, A.Taninaka, T.Yokawa, H.Shinohara. *J.Am. Chem.Soc.* 2003, **125**, 4391 – 4397
6. PP.Fatouros, MD.Shultz. 2013, **8(11)**, 1853-64
7. K.Akiyama, T.Hamano, Y.Nakanishi, E.Takeuchi, S.Noda, Z.Wang. et al. *J.Am.Chem.Soc.* 2012, **134**, 9762-9767
8. MH.Olmstead, A.de Bettencourt-Dias, J.C.Duchamp, S. Stevenson, D.Marcu, H.C.Dorn. et al. *Angew.Chem.Int.Ed.* 2001, **40**, 1223-25
9. S.Yang, L.Zhang, W.Zhang, LA.Dunsch. *Chem.Eur.J.* 2010, **16**, 12398-12405
10. S.Stevenson, MC.Thompson, HL.Coumber, MA.Mackey, CE.Coumbe, JP.Phillips. *J.Am.Chem.Soc* 2007, **129**, 16257-12662
11. S.Stevenson, MA.Mackey, MC.Thompson, HL.Coumbe, P.Madasu, CE.Coumbe. et al. *Chem Commun.* 2007, 4263–4265
12. M.Keidar, A.Shashurin, J.Li, O.Volotskova, M.Kundrapu, TS.Zhuang. *J Phys D: Appl Phys* 2011, **44**, 174006-174012
13. C.Journet, WK.Maser, P.Bernier, A.Loiseau, M.Lamy de la Chapelle, S.Lefrant. et al. *Nature* 1997, **388**, 756-758
14. X.Lv, F.Du, Y.Ma, O.Wu, Y.Chen. *Carbon* 2005, **43**, 2020
15. S.Iijima. *Nature* 1991, **354**, 56 – 58
16. W.Kratschmer, LD.Lamb, K.Fostiropoulos, DR.Huffman. *Nature* 1990, **347**, 354-358
17. MA.Pimenta, G.Dresselhaus, MS.Dresselhaus LG.Cancado, A.Jorio, R.Saito. *Phys Chem Chem Phys* 2007, **9**, 1276–1291
18. A.Chuvilin, U.Kaiser, E.Bichoutskaia, NA.Besley, AN.Khlobystov. *Nature Chem* 2010, **2**, 450-453
19. Z.Li, Z.Cheng, R.Wang, Q.Li, Y.Fang. *Nano Letters* 2009, **9(10)**, 3599-3602
20. B.L'Vov, AV.Novichikhin. *Spectrochimica Acta B.* 1995, **50**, 1459-1468
21. Z.Ding, W.Martens, RL.Frost. *J.Mater.Sci.Lett* 2002, **21**, 1415-1417
22. KH.Stern. *J.Phys.Chem.Ref.Data* 1972, **1**, 747-772
23. IV.Morozov, KO.Znamenkov, YM.Korenev, OA.Shlyakhtin. *Thermochimica Acta* 2003, **403**, 173-179
24. I.Beilis, M.Keidar, RL.Boxman, S.Goldsmith, J.Heberlein, E.Pfender. *J.Appl.Phys* 1999, **86**, 114-119
25. H.Yang, C.Lu, Z.Liu, H.Jin, Y.Che, MM.Olmstead, AL.Balch. *J.Am.Chem.Soc.* 2008, **130**, 17296-17300
26. Z.Wang, Y.Nakanishi, S.Noda, H.Niwa, J.Zhang, R.Kitaura, H.Shinohara. *Angew Chem Int Ed* 2013, **52**, 11770-11774
27. HD.Beckhaus, S.Verevkin, C.Riichardt, F.Diederich, C.Thilgen, HU.ter Meer, H.Mohn, W.Miller. *Angew Chem Int Ed* 1994, **33**, 996-998
28. S.Stevenson, G.Rice, T.Glass, K.Harich, F.Cromer, MR.Jordan. et al. *Nature* 1999, **401**, 55-57
29. S.Yang, AA.Popov, C.Chen, L.Dunsch. *J.Phys.Chem.C.* 2009, **113**, 7616-7623
30. SF.Yang, S.Troyanov, A.Popov, M.Krause, L.Dunsch. *J.Am.Chem.Soc.* 2006, **128**, 16733-16739
31. PW.Dunk, M.Mulet-Gas, Y.Nakanishi, NK.Kaiser, A. Rodriguez-Forte, H.Shinohara. JM.Poblet, AG.Marshall, HW.Kroto. *Nature Communications* 2014, **5**, 5844-5852
32. S.Yang, C.Chen, F.Liu, Y.Xie, F.Li, M.Jiao et al. *Scientific Reports.* 2013, **3**, 1487-1482
33. F.Liu, S.Wang, J.Guan, T.Wei, M.Zeng, S.Yang. *Inorg.Chem.* 2014, **53**, 5201–5205
34. YZ.Tan, RT.Chen, ZL.Liao, J.Li, F.Zhu, X.Lu. et al. *Nat.Comm.* 2011, **2**, 420-426
35. A.Hirsch, M.Brettreich. "Fullerenes: Chemistry and Reactions" John Wiley & Sons
36. LPF.Chibante, A.Thess, JM.Alford, MD.Diener, RE.Smalley. *J Phys Chem* 1993, **97**, 8696-8700
37. Z.Shi, Y.Lian, X.Zhou, Z.Gu, Y.Zhang, S.Iijima. et al. *Carbon* 1999, **37**, 1449–1453
38. M.Keidar, AM.Waas. *Nanotechnology* 2004; **15**: 1571-1575
39. R.Taylor. *Interdiscip Sci Rev* 1992, **17**, 161–170.
40. J.Zhang, FL.Bowles, DW.Bearden, WK.Ray, T.Fuhrer, Y.Ye et al. *Nature Chemistry* 2013, **5**, 880-885
41. SS.Meysami, F.Dillon, AA.Koós, Z.Aslam, N.Grobert. *Carbon* 2013, **5**, 151–158
42. RJ.Nicholls, J.Britton, SS.Meysami, AA.Koós, N.Grobert. *Chem. Commun* 2013, **49**, 10956-10958
43. SS.Meysami, AA.Koós, F.Dillon, N.Grobert. *Carbon* 2013, **58**, 159–169
44. C.Deck, K.Vecchio. *Carbon* 2006, **44(2)**, 267-275
45. W.Zhou, Z.Han, J.Wang, Y.Zhang, Z.Jin, X.Sun X et al. *Nano Letters* 2006, **6(12)**, 2987-2990
46. Y.Gogotsi. Carbon nanomaterials, second edition (advanced materials and technologies) Volker Presser. CRS Press, **2013**
47. M.Swierczewska, I.Rusakova, B.Sitharaman. *Carbon* 2009, **47(13)**, 3139–3142
48. Y.Saito, M.Okuda, T.Yoshikawa, Kasuya, Y.Nishina. *J.Phys.Chem.* 1994, **98**, 6696-6698
49. H.Cao, R. Li, J.Xue, H.Li, X.Wang, X.Bin *Carbon* 2009, **47**, 1543 –1548